

# Feature Article

Application

## Non-Destructive Evaluation of SiC wafer for Power Device

Defect detection in  $\mu\text{m}\sim\text{nm}$  scale using optical analytical technique

Nobuyuki NAKA

Tomoya SHIMIZU

Hiroki BABA

Tomoko NUMATO

Junichi AOYAMA

Shogo AWATA

Tomoaki HATAYAMA

Power devices using Silicon Carbide (SiC) are already commercialized and are moving into mass production, but commercial SiC wafers have several types of defects. It is important to have techniques for analyzing a variety of defects, because these defects decrease the yield ratio of SiC devices. In this paper, we did complex analysis on sub-millimeter- and nanometer-scale defects and stress in epitaxial/bulk SiC wafers. The laser scattering method can detect submicron-sized defects on the entire surface of a 4-inch (10.16 cm) wafer in about 3 minutes. Our original Cathode Luminescence (CL) imaging system can evaluate nanometer-sized crystal defects using a sub-millimeter-scale panchromatic image acquired in a short time, and Photo Luminescence (PL) lifetime measurements help us understand carrier lifetime. Furthermore, we show that Raman spectroscopy can evaluate stress distribution around defects detected in CL images in a non-destructive manner.

### Introduction

Silicon Carbide (SiC) has excellent heat resistance and electrical characteristics. Silicon has been in general use in semiconductor devices, and SiC is expected to be applied to devices that need heat resistance or large current operation, such as electric vehicles or smart grids, and also to power devices for equipment that requires a high conversion efficiency<sup>[1]</sup>. However, as shown in Figure 1, SiC wafers in the market have a high density of crystal defects, such as stacking defects, Basal Plane

Dislocation (BPD), and Threading Dislocation (TD). These defects can cause the insulation to be destroyed while the device is in operation, so SiC wafers have essentially not been applied to things like metal-oxide-silicon field-effect transistors. To reduce the crystal defect density and use SiC wafers on various types of devices, we need to optimize the wafer manufacturing conditions and device manufacturing conditions by applying the detailed defect evaluation results to the crystal growth process.

Our objective was to provide new evaluation equipment and techniques for improving the crystal quality of SiC wafers and device production yield. It is known that light can be used as an effective analysis technology in evaluating SiC wafers, and defects in particular<sup>[1]</sup>. The HORIBA Group has many optical analysis technologies, and HORIBA may be able to provide various analysis technologies to meet the requirements for evaluating SiC wafers. This report introduces the results of using various non-destructive analysis methods to evaluate SiC wafer defects, particularly defects in 4H-SiC wafers with

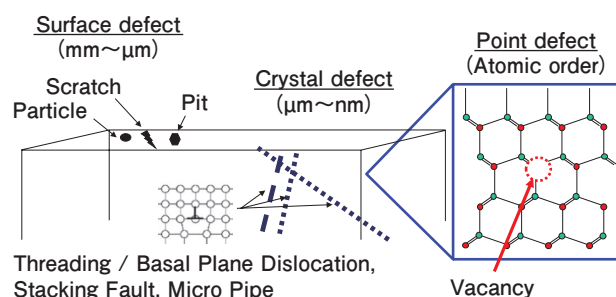


Figure 1 Schematic diagram of defect type in SiC wafer.

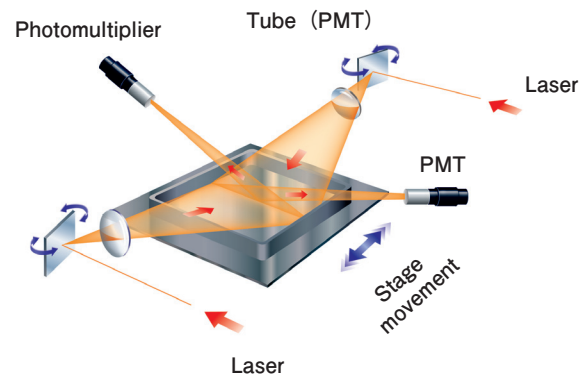


Figure 2 Apparatus and Optical configuration of particle/defect detection (PR-PD2).

epitaxial film and bulk wafers. Specifically, laser scattering defect detection technology was used to measure mm- to  $\mu\text{m}$ -order surface defects and abnormalities, CathodeLuminescence (CL) was used for  $\mu\text{m}$ - to sub- $\mu\text{m}$ -order crystal defects, PhotoLuminescence (PL) lifetime measurements were used for average atomic-level defects such as lattice defects and carrier concentration, and Raman spectroscopy was used to evaluate stress in crystal defect areas. We obtained effective data for observing nm-order dislocation defects using CL imaging measurements for SiC epitaxial film and bulk wafers, for which there have been few evaluation reports using non-destructive defect evaluation methods up to this point. For all these measurement methods, there was no need to prepare special samples, and using various combinations of the methods made it possible to evaluate various scales of crystal defects in a non-destructive manner.

## Evaluation Methods and Measurement Samples

### Evaluation methods

#### Detecting defects using laser scattering

In particular, we applied the optical system of the inspection measuring device (PR-PD Series)<sup>[2]</sup> made by HORIBA, Ltd. that we developed to detect abnormalities and defects in reticles/masks used in semiconductor lithography processes, and used this optical system to measure and inspect defects in SiC wafers. Figure 2 shows the appearance of the PR-PD2. This device uses an argon laser with a wavelength of 488 nm. An f $\theta$  lens is used to make this laser light converge on the measurement surface, a galvanometer is used to do a primary scan (Y direction) on the measurement surface, and at the same time the unit

moves at a constant speed in the direction that is perpendicular to the scan (X direction). These operations are used to measure the entire object. At this time, if there is an object on the measurement surface that scatters the laser light, scattered light is generated, but a condenser lens is used to condense the scattered light into a photomultiplier tube. The PR-PD2 detects changes in the photomultiplier tube's electrical signals as abnormalities or defects. The optical system used for these measurements is capable of detecting pin holes of 0.3  $\mu\text{m}$  or less formed in chromium film on a glass surface.

### Cathodeluminescence (CL)

Cathodeluminescence (CL) is a phenomenon in which a substance emits light when it is excited by an electron beam. This CL light can be used to evaluate the structure of substances and crystal defects when a spectroscope is used to measure the spectrum<sup>[3]</sup>. The hardware is generally composed of an optical condenser system inside a vacuum chamber in the sampling chamber of a scanning electron microscope (SEM), with a spectroscope and detector attached to the chamber port. CL mapping measurements that use an automatic sample drive stage use the fact that the strength of the light emission spectra is different in defect areas and non-defect areas to specify secondary defect areas. Figure 3 shows the Imaging CL

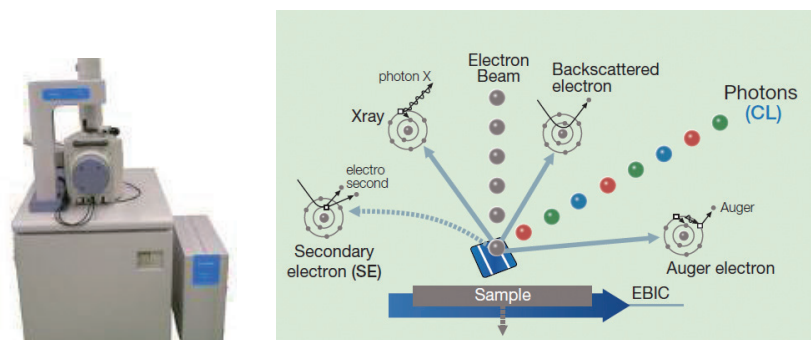


Figure 3 Imaging CL system (DF-100) and light emitting by electron beam irradiation.

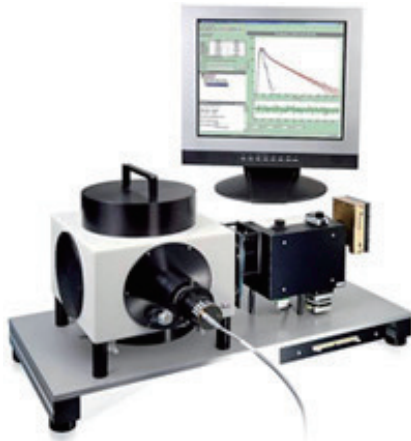


Figure 4 Apparatus of fluorescence life time measuring system (FluoroCube 5000U).

DF-100 made by HORIBA, Ltd., which is the CL equipment used for the work in this paper. This CL equipment uses the differences in light emission strength in defect areas and non-defect areas to evaluate defect locations and types in a short time, by obtaining panchromatic images (detecting all the CL light without doing spectroscopy) at higher speeds than CL equipment for measuring spectra. The equipment can do this because it uses an electrical system with improved signal processing speed to set the electron beam irradiation time per pixel via electronic scanning to 10 ns or less. Also, shortening the electron beam irradiation time controls carrier diffusion and decreases the light emission range, which makes it possible to take measurements with high spatial resolution. It depends on the measurement conditions, but this device can measure an 0.5 mm angle range at a sub- $\mu\text{m}$ -order of spatial resolution in some tens of minutes. These measurements were taken at an acceleration voltage of 10 kV, current of 1.0 nA, and room temperature. The CL spectrum measurements were taken using the MP-Micro-S made by HORIBA, Ltd., which can take spectroscopy measurements.

### Photoluminescence (PL) lifetime

Electron hole/pair recombination lifetime measurements that can be obtained by measuring the changes in PL



Figure 5 Apparatus of Raman scattering measuring system (LabRAM HR Evolution).

strength time when excited by picosecond laser light are effective in evaluating crystal properties of semiconductors, such as residual carrier concentration inside the semiconductor and defect density. For PL lifetime measurements, we used a FluoroCube 5000U made by HORIBA Jobin Yvon, which uses a time-to-amplitude converter system. Figure 4 shows the appearance of this device. The time-to-amplitude converter system starts when a pulse light is generated from the light source, and stops when the PL photons generated by excited photons reach the detector. It then converts the electric charge accumulated during that time to voltage, makes a histogram of the time, finds a fitting curve that corresponds to the emission damping curve, and calculates the PL lifetime. The measurements in this paper used a pulse laser (355 nm wavelength, 592 ps pulse width) as the light source, and were taken at room temperature under conditions deemed as low injection.

### Raman spectroscopy

The Raman spectroscopy method is a method for analyzing the structure and nature of substances by measuring the Raman scattered light obtained by spectroscopy or crystal vibration. When the laser is aimed at a substance as excitation light, the phenomenon in which light at a different wavelength than the wavelength (energy) of the laser light is discharged is called Raman scattering. If we use a spectroscope to measure the spectrum of this scattered light, we can get information about the spectroscopic lattice and structure of the substance. For semiconductors, the Raman spectrum has a relatively sharp peak, and the stress and strain inside the substance from this peak shift location can be evaluated. Figure 5 shows the appearance of the LabRAM HR Evolution made by HORIBA Jobin Yvon, which is a laser-based microscopic Raman spectroscopy device.

The measurements were taken with an argon laser (488 nm) as the excitation light, at room temperature, with a rear scattering configuration.

Table 1 Main specification of SiC wafer (Size : 4inch).

	Wafer type	Surface	Crystal axis	Dopant conc. ( $\text{cm}^{-3}$ )	Polished surface	Thickness ( $\mu\text{m}$ )
Sample A	4H-SiC Epitaxial film on bulk	Si	[11-20] 8° off	$4 \times 10^{14}$	One side	20
Sample B	4H-SiC bulk	Si	[11-20] 4° off	$>1 \times 10^{18}$	Both side	–
Sample C	4H-SiC bulk	Si	[11-20] 8° off	$>1 \times 10^{18}$	One side	–

### Measurement samples

Sample A was a 4H-SiC epitaxial wafer, and Samples B and C were 4H-SiC epitaxial wafers. The wafer specifications are shown in Table 1. All the wafers are 4 inches (10.16 cm).

### Results and Conclusion

#### Evaluating surface defects and crystal defects

Figure 6 shows the defect measuring results using the PR-PD2 laser scattering defect inspection device. This device measured all surfaces of the Sample B bulk wafer in 3 minutes. As you can see in Figure 6, defects and abnormalities (micropipes, particles, and scratches) of a size from a few  $\mu\text{m}$  to some tens of  $\mu\text{m}$  were detected, and a total of 73 defects and abnormalities were detected. Figure 7 shows the Sample C bulk wafer defect measurement results from the PR-PD2 and the CL imaging measurement results. In addition to Sample B defects, we observed surface pits that were a few  $\mu\text{m}$  in size. We also measured the CL images around the pits, and tried to observe defects in the wafer surface layer. As you can see in Figure 7, the device not only found surface defects, but also found many line-shaped defects inside the wafer around the pits, whose starting points were pits that were not observed using SEM imaging. Also, in ranges where SEM imaging did not find any defects in the same wafer, CL imaging showed lines and defects that are probably the grain boundary. This type of defect evaluation using CL imaging can be done by observing the changes in spectrum strengths, as shown below.

Figures 8(a) and 8(b) show the CL imaging measurement results and CL spectrum of epitaxial wafer Sample A. As shown in Figures 8(a) and 8(b), in ranges where SEM imaging did not find anything, CL imaging showed trapezoidal-shaped images. We speculate that this is a stacking defect that exists near the surface. As shown in Figure 8(b), based on this CL spectrum range, in the non-defect range, we found strong light emissions that we speculate were caused by band edge light emission near 385 nm, residual impurities starting at 500 nm, and point defects. In the stacking defect range, we found that the spectrum strength was weak. More specifically, we can say that these spectrum strength differences are obtained as defect images.

Figures 9(a) and 9(b) show CL imaging for epitaxial wafer Sample A and the bright field image after molten salt KOH etching. The etch-pit method (observing the surface after KOH etching) is known as being a high-accuracy method for evaluating defects on SiC wafers<sup>[4]</sup>.

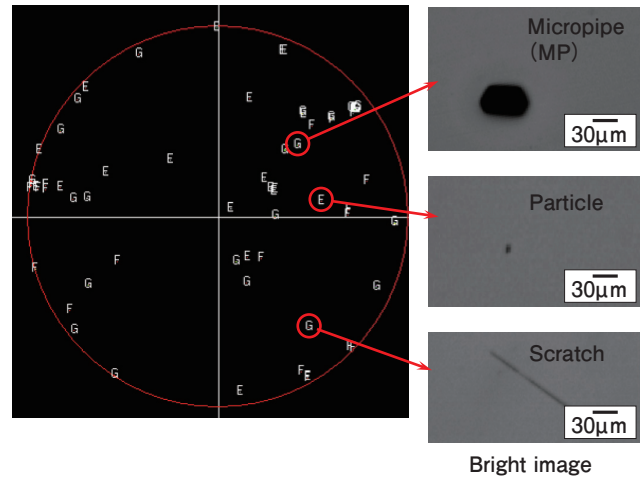


Figure 6 Particle/Defect detection result of Sample B (Bulk wafer).

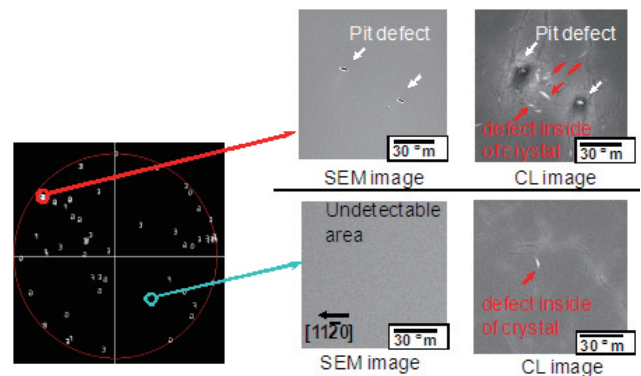
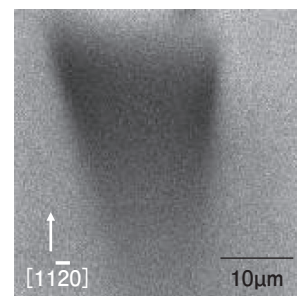
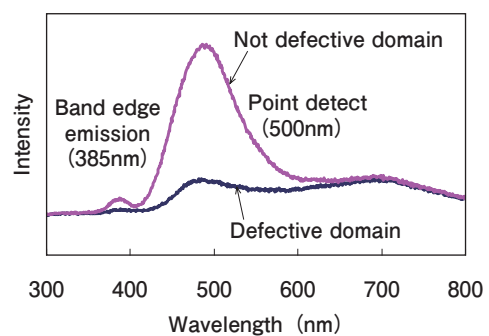


Figure 7 Particle/Defect detection result and CL image of Sample C (Bulk wafer).

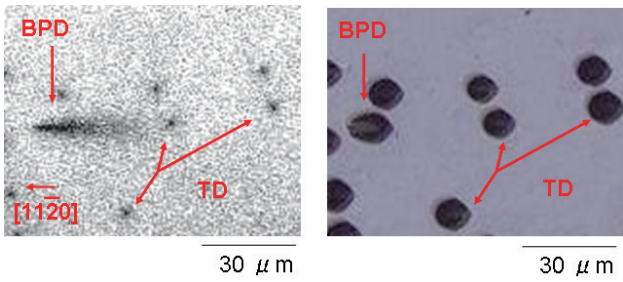


(a) Panchromatic CL image

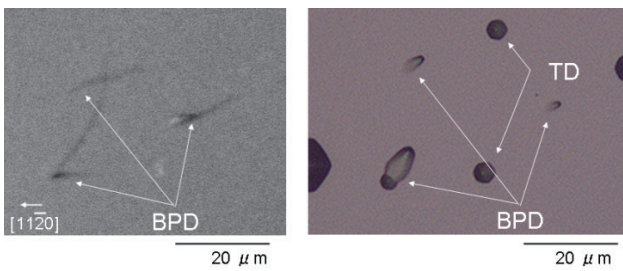


(b) CL spectrum

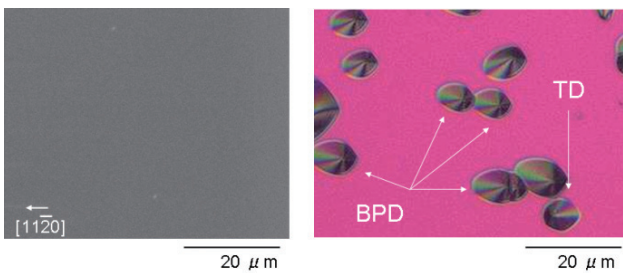
Figure 8 CL image and CL spectrum for stacking fault of Sample A (Epitaxial wafer).



(a) Panchromatic CL image (b) Optical image after KOH etching  
Figure 9 Defect evaluation result of Sample A (Epitaxial wafer).



(a) Panchromatic CL image (b) Optical image after KOH etching  
Figure 10 Defect evaluation result of Sample B (Bulk wafer).



(a) Panchromatic CL image (b) Optical image after KOH etching  
Figure 11 Defect evaluation result of Sample C (Bulk wafer).

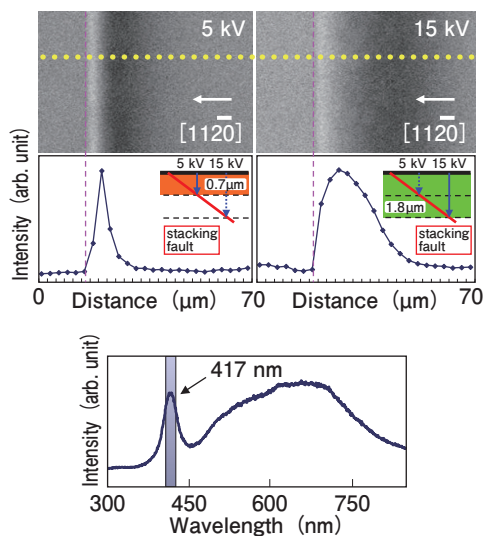


Figure 12 Evaluation result in depth direction for stacking fault of Sample B (Bulk wafer).

In smooth ranges where scratches, etc. were not observed using SEM imaging, CL imaging found dark lines and dark spots. At the starting point of the dark lines found using CL imaging, we found shell pits in the bright field image after etching. Also, in the same location as the dark spots found using CL imaging, we found hexagonal pits in the bright field image after etching. It has been reported that shell pits that are formed by molten salt KOH etching correspond to Basal Plane Dislocation (BPD), and hexagonal pits correspond to Threading Dislocation (TD)<sup>[4]</sup>. We found that the dark lines from CL imaging correspond to BPD, and the dark spots correspond to TD. Up until now, PL imaging measurements have been used to observe and report dislocation defects<sup>[5]</sup>, but CL imaging measurements have not been used to observe and report dislocation defects<sup>[6]</sup>. In these CL imaging measurements, improving the signal processing speed during measurements and shortening the electron beam irradiation time means that less of the carrier that diffuses in the electron beam irradiation area is used and the light emission range is smaller. Therefore, this probably enabled us to observe the discoloration defects (BPD and TD) at a high contrast.

Figures 10(a) and 10(b) show the CL imaging for the Sample B bulk wafer and the bright field image after molten salt KOH etching. In smooth ranges where scratches, etc. were not observed using SEM imaging, CL imaging found dark lines. At the starting point of the dark lines found using CL imaging, we found shell pits in the bright field image after etching. More specifically, these dark lines correspond to BPD. These CL imaging measurements make it possible to observe BPD at high contrast in SiC bulk wafers in a non-destructive manner, a subject about which there have been few reports. Also, in the same location as the dark spots found using CL imaging, we found hexagonal pits in the bright field image after etching. More specifically, TD was not observed.

Figures 11(a) and 11(b) show the CL imaging for the Sample C bulk wafer and the bright field image after molten salt KOH etching. In ranges where nothing was observed using SEM imaging and CL imaging, BPD and TD were observed in the bright field image. Up until now, the high-density point defect  $Z_{1/2}$  center was the cause of a decreased carrier lifetime, and it has been reported that this caused a contrast decrease in defect images using PL imaging measurements<sup>[6]</sup>. In the CL imaging measurements this time, bulk wafer Samples B and C had a high concentration of impurities and a short carrier lifetime, so the dislocation defect imaging contrast was low, and we speculate that defects exist that are difficult to observe using CL measurements.

Next are the CL measurement results that investigated the depth direction. Figure 12 shows the bulk wafer Sample B CL imaging measurement results with the acceleration voltage of the electron beam changed and CL spectrum for the wafer. Figure 12 shows CL imaging at an acceleration voltage of 5 kV and 15 kV, and the primary strength distribution of the spectrum<sup>[7]</sup> near 417 nm with high strength in the stacking defect range. We investigated the electron beam penetration depth based on the length in the dark area direction (112-0), and found that the depth is 0.7 μm when the acceleration voltage is 5 kV, and 1.8 μm when the acceleration voltage is 15 kV. More specifically, we can say that it is possible to control the depth direction obtained by changing the acceleration voltage, and that this data shows that CL measurements are effective in observing sub-μm-order surface layer defects.

We found that laser scattering defect detection technology and CL measurement technology are effective as non-destructive methods for evaluating SiC wafer defects. In particular, using sub-μm-order spatial measurement resolution with this CL measurement device enables us to accurately specify the crystal defect location and type. We also found that the defect types that can be clearly detected differ between epitaxial wafers and bulk wafers. This is probably because of differences in the concentration of impurities, and we need to combine this with evaluating the concentration of impurities using another method.

### Evaluating carrier lifetime

To investigate CL emission differences based on the wafer differences in the previous section, namely the concentration of impurities, we evaluated the carrier lifetime using PL lifetime measurements. Figure 13 shows the PL spectra of Samples A, B, and C. Sample A mainly had band edge light emission at 390 nm. Samples B and C also had band edge light emission, and also had a broad spectrum of long wavelengths, with 500 nm as the peak. Figure 14 shows the PL lifetime measurement results for the 390-nm band edge light emission of Samples A, B, and C. Based on Figure 14, we can see that the lifetime components clearly differ between samples. When we calculated a 1/e carrier lifetime in the range inside the dotted line, Sample A was 300 ns, Sample B was 100 ns, and Sample C was 10 ns. These measurements were taken under low injection conditions, and the values we obtained are deemed to be minority carrier lifetimes. Klein et al. have reported on the correlation between carrier lifetime and point defect  $Z_{1/2}$

center density. We speculate that the  $Z_{1/2}$  center density is high because the carrier lifetime was significantly shorter in Sample C (10 ns) than in Sample A (300 ns)<sup>[8]</sup>.

### Evaluating stress around defect areas

This section will discuss the results of using Raman spectroscopy to evaluate stress in defect areas found using CL imaging. Figure 15 shows the Raman spectrum of 4H-SiC bulk wafer B. The peak shift of the Raman spectrum has correlation with the stress applied to the lattice. If we find the phonon (FTO<sub>2/4</sub>) peak shift amount, we can find the change in stress inside the crystal<sup>[4]</sup>.

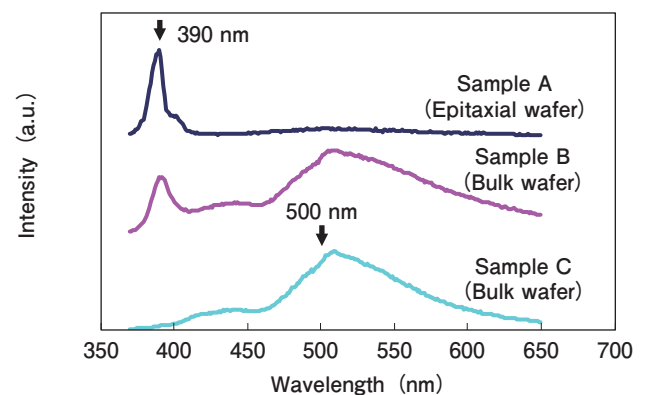


Figure 13 Fluorescence spectrum of Sample A, B and C.

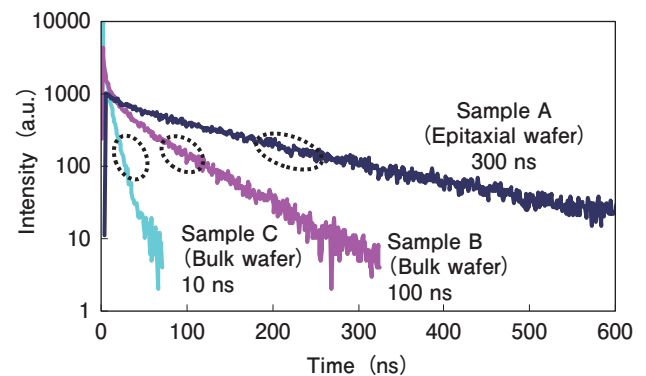


Figure 14 Lifetime curve of Sample A, B and C.

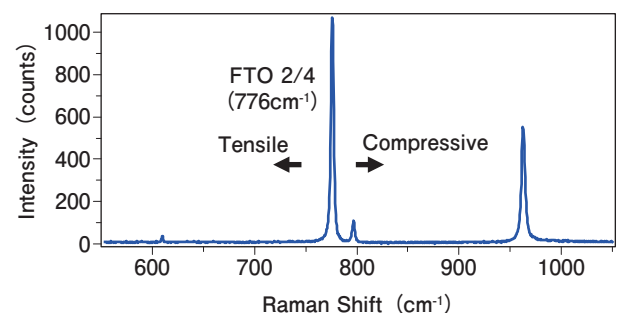
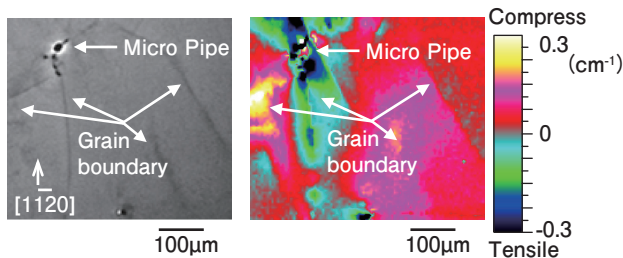


Figure 15 Raman spectrum of Sample B (Bulk wafer).



(a) Panchromatic CL image (b) Raman peak shift map

Figure 16 CL image and stress evaluation result of Sample B (Bulk wafer)

Figures 16(a) and 16(b) show the phonon ( $FTO_{2/4}$ ) peak shift distribution obtained via Raman spectroscopy measurements using CL imaging on bulk wafer Sample B in this range. Based on the CL imaging in Figure 16(a), in Sample B, we found a defect associated with a hole with a diameter of 10  $\mu\text{m}$  or more, and line-shaped defects in the surrounding area. The defects associated with the hole are micropipes, and the line-shaped defects are probably the grain boundary<sup>[9]</sup>. If we look at Figure 16(b), we can see that there has been a change in the peak phonon frequency in the location that corresponds to the grain boundary area. Strong tensile stress and compressive stress occur near the micropipe, and we can say that there is a sharp stress distribution in the grain boundary near the micropipe. These results suggest that even in ranges where SEM imaging does not detect defects, stress may be distributed inside the wafer if there is a defect inside the wafer.

## Summary

The HORIBA Group has evaluated SiC wafer defects using various types of optical analysis technology. To really introduce SiC wafers into the market, it will be necessary to have even more advanced technology, defect inspection technology in particular. This paper introduced evaluation at the wafer level. From the perspective of power devices that require high reliability, evaluating different properties and detecting defects at the device level in silicon devices will be an important technology in the future. The HORIBA Group hopes to link SiC research and development to develop technology that can contribute to the real introduction of SiC wafers into the market, as well as contribute to the evolution of power devices.

## References

- [ 1 ] Hiroyuki Matsunami, et al., Technology of Semiconductor SiC and Its Application, (Business & Technology, 2011).
- [ 2 ] Toyoki Kanzaki, *Readout (HORIBA Technical Reports)*, **30**, 92 (2005).
- [ 3 ] R. Sugie, et al., *Mater. Sci. Forum*, 600-603, **353** (2009).
- [ 4 ] H.Matsuhata, et al., *Mater. Sci. Forum*, 600-603, **309** (2009).
- [ 5 ] G.Feng, et al., *J. Appl. Phys.*, **110**, 33525 (2011).
- [ 6 ] S.I.Maximenko, et al., *Appl. Phys. Lett.*, **94**, 92101 (2009).
- [ 7 ] B.Chen et al., *Appl. Phys. Lett.*, **93**, 33514 (2008).
- [ 8 ] P.B.Klein, et al., *Appl. Phys. Lett.*, **88**, 52110 (2006).
- [ 9 ] M.Tajima, et al., *Appl. Phys. Lett.*, **86**, 61914 (2005)



### Nobuyuki NAKA

Manager  
Scientific & Semiconductor Instruments R&D Dept.  
Application R&D Center  
HORIBA, Ltd.  
Ph. D.



### Tomoya SHIMIZU

Scientific & Semiconductor Instruments R&D Dept.  
Application R&D Center  
HORIBA, Ltd.



### Hiroki BABA

Scientific & Semiconductor Instruments R&D Dept.  
Application R&D Center  
HORIBA, Ltd.



### Tomoko NUMATO

Scientific & Semiconductor Instruments R&D Dept.  
Application R&D Center  
HORIBA, Ltd.



### Junichi AOYAMA

Advanced R&D Center  
HORIBA, Ltd.  
Ph. D.



### Shogo AWATA

Advanced R&D Center  
HORIBA, Ltd.  
Ph. D.



### Tomoaki HATAYAMA

Nara Institute of Science and Technology  
Ph. D.